Letter

Constraints on the symmetry energy from PREX-II in the multimessenger era

Tong-Gang Yue,[1] Lie-Wen Chen,[1,*] Zhen Zhang,[2] and Ying Zhou[3]

[1]*School of Physics and Astronomy, Shanghai Key Laboratory for Particle Physics and Cosmology, and Key Laboratory for Particle Astrophysics and Cosmology (MOE), Shanghai Jiao Tong University, Shanghai 200240, China*

[2]*Sino-French Institute of Nuclear Engineering and Technology, Sun Yat-sen University, Zhuhai 519082, China*

[3]*Quantum Machine Learning Laboratory, Shadow Creator Inc., Shanghai 201208, China*

(Received 15 February 2021; revised 9 February 2022; accepted 24 May 2022; published 8 June 2022)

The neutron skin thickness $\Delta r_{\rm np}$ of heavy nuclei is essentially determined by the symmetry energy density slope $L(\rho)$ at $\rho_c = 0.11$ fm$^{-3} \approx 2/3\rho_0$ (ρ_0 is nuclear saturation density), roughly corresponding to the average density of finite nuclei. The PREX collaboration recently reported a model-independent extraction of $\Delta r_{\rm np}^{208} = 0.283 \pm 0.071$ fm for the $\Delta r_{\rm np}$ of ^{208}Pb, suggesting a rather stiff symmetry energy $E_{\rm sym}(\rho)$ with $L(\rho_c) \geqslant 52$ MeV. We show that the $E_{\rm sym}(\rho)$ cannot be too stiff and $L(\rho_c) \leqslant 73$ MeV is necessary to be compatible with (1) the ground-state properties and giant monopole resonances of finite nuclei, (2) the constraints on the equation of state of symmetric nuclear matter at suprasaturation densities from flow data in heavy-ion collisions, (3) the largest neutron star (NS) mass reported so far for PSR J0740+6620, (4) the NS tidal deformability extracted from gravitational wave signal GW170817, and (5) the mass-radius of PSR J0030+045 measured simultaneously by NICER. This allows us to obtain $52 \leqslant L(\rho_c) \leqslant 73$ MeV and $0.212 \leqslant \Delta r_{\rm np}^{208} \leqslant 0.271$ fm and further $E_{\rm sym}(\rho_0) = 34.3 \pm 1.7$ MeV, $L(\rho_0) = 83.1 \pm 24.7$ MeV, and $E_{\rm sym}(2\rho_0) = 62.8 \pm 15.9$ MeV. A number of critical implications on nuclear physics and astrophysics are discussed.

DOI: 10.1103/PhysRevResearch.4.L022054

Introduction. The Lead Radius Experiment (PREX) collaboration recently reported a model-independent extraction of $\Delta r_{\rm np}^{208} = 0.283 \pm 0.071$ fm [1] for the neutron skin thickness (the difference between the rms radii of the neutron and proton distributions, $\Delta r_{\rm np} \equiv r_n - r_p$) of ^{208}Pb by combining the original PREX result [2] with the new PREX-II measurement [1]. This updated result (hereafter referred to as simply "PREX-II") reaches a precision close to 1% for r_n, much more precise than the original $\Delta r_{\rm np}^{208} = 0.33^{+0.16}_{-0.18}$ fm [2]. In PREX, the neutron density distribution in ^{208}Pb is determined by measuring the parity-violating electroweak asymmetry in the elastic scattering of polarized electrons off ^{208}Pb and thus is free from the strong interaction uncertainties. Since the proton is charged and its distributions are well determined, the $\Delta r_{\rm np}^{208} = 0.283 \pm 0.071$ fm may represent the cleanest and most accurate $\Delta r_{\rm np}^{208}$ so far although the more precise measurement has been planned at MESA [3]. The coherent elastic neutrino-nucleus scattering [4] provides another clean way to extract the $\Delta r_{\rm np}$, but the current uncertainty is too large [5,6]. The 0.283 ± 0.071 fm means a rather thick $\Delta r_{\rm np}^{208}$, significantly larger than those extracted from other approaches that suffer from the uncertainties of the strong interaction (see, e.g., Ref. [7] for a recent review).

Besides its fundamental importance for nuclear structure, the $\Delta r_{\rm np}$ has been identified as an ideal probe on the symmetry energy $E_{\rm sym}(\rho)$—a key but poorly known quantity that encodes the isospin dependence of nuclear matter equation of state (EOS) and plays a critical role in many issues in nuclear physics and astrophysics [8–13]. Indeed, it has been established [14–19] that the $\Delta r_{\rm np}$ exhibits a strong positive linear correlation with the symmetry energy density slope $L(\rho)$ at nuclear saturation density $\rho_0 \approx 0.16$ fm^{-3}, i.e., $L \equiv L(\rho_0)$. An even stronger correlation is found between the $\Delta r_{\rm np}$ of heavy nuclei and the $L(\rho)$ at a subsaturation cross density $\rho_c = 0.11$ fm$^{-3} \approx 2/3\rho_0$ [20], roughly corresponding to the average density of finite nuclei, i.e., $L_c \equiv L(\rho_c)$. Furthermore, the $L(\rho)$ around ρ_0 strongly influences the mass-radius (M-R) relation and tidal deformability of neutron stars (NSs) and thus provides a unique bridge between atomic nuclei and NSs [21–24].

The large value of $\Delta r_{\rm np}^{208} = 0.283 \pm 0.071$ fm suggests a very stiff $E_{\rm sym}(\rho)$ [a large $L(\rho)$] around ρ_0, which generally leads to a very large NS radius and tidal deformability. However, an upper limit of $\Lambda_{1.4} \leqslant 580$ [25] for the dimensionless tidal deformability of $1.4M_\odot$ NS has been obtained from the gravitational wave signal GW170817, which requires a relatively softer $E_{\rm sym}(\rho)$. In addition, the heaviest NS with mass $2.14^{+0.10}_{-0.09}M_\odot$ for PSR J0740+6620 [26] also strongly limits the $E_{\rm sym}(\rho)$ [24], especially under the constraints on the EOS of symmetric nuclear matter (SNM) at suprasaturation densities from flow data in heavy-ion collisions (HIC) [27], which is relatively soft and strongly restricts the NS maximum mass $M_{\rm max}$ [23,24,28]. Furthermore, two independent simultaneous M-R determinations from NICER [29,30] for

*Corresponding author: lwchen@sjtu.edu.cn

PSR J0030+0451 with mass around $1.4M_\odot$ has been obtained, further constraining the $E_{\rm sym}(\rho)$. Given the rich multimessenger data, it is extremely important to develop a unified framework that can simultaneously describe the finite nuclei and NSs which involve a very large density range. Actually, serious tension between $\Delta r_{\rm np}^{208} = 0.283 \pm 0.071$ fm and the limits from GW170817 and NICER has been observed in a covariant density functional study [31].

In this work, within a single unified framework of the extended Skyrme-Hartree-Fock (eSHF) model [32,33] which includes momentum dependence of effective many-body forces, we find the L_c cannot be larger than 73 MeV under the constraints from GW170817, NICER, the NS mass $2.14^{+0.10}_{-0.09}M_\odot$, flow data in heavy-ion collisions, and the data of ground-state properties and giant monopole resonances (GMR) of finite nuclei. Our findings produce an upper limit of $\Delta r_{\rm np}^{208} \leqslant 0.271$ fm, and this together with the $\Delta r_{\rm np}^{208} = 0.283 \pm 0.071$ fm lead to stringent constraints of $0.212 \leqslant \Delta r_{\rm np}^{208} \leqslant 0.271$ fm and correspondingly $52 \leqslant L_c \leqslant 73$ MeV, which have a number of critical implications in nuclear physics and astrophysics.

Model and method. The EOS of nuclear matter at density $\rho = \rho_n + \rho_p$ and isospin asymmetry $\delta = (\rho_n - \rho_p)/\rho$ with $\rho_n(\rho_p)$ denoting the neutron(proton) density, defined by the binding energy per nucleon, can be expressed as

$$E(\rho, \delta) = E_0(\rho) + E_{\rm sym}(\rho)\delta^2 + \mathcal{O}(\delta^4), \tag{1}$$

where $E_0(\rho) = E(\rho, \delta = 0)$ is SNM EOS and $E_{\rm sym}(\rho) = \frac{1}{2!}\frac{\partial^2 E(\rho,\delta)}{\partial \delta^2}|_{\delta=0}$ is the symmetry energy. At ρ_0, the $E_0(\rho)$ can be expanded in $\chi = (\rho - \rho_0)/(3\rho_0)$ as $E_0(\rho) = E_0(\rho_0) + \frac{1}{2!}K_0\chi^2 + \frac{1}{3!}J_0\chi^3 + \mathcal{O}(\chi^4)$, in terms of incompressibility K_0 and skewness J_0. The $E_{\rm sym}(\rho)$ can be expanded at a reference density ρ_r in terms of the slope parameter $L(\rho_r)$ and the curvature parameter $K_{\rm sym}(\rho_r)$ as $E_{\rm sym}(\rho) = E_{\rm sym}(\rho_r) + L(\rho_r)\chi_r + \frac{1}{2!}K_{\rm sym}(\rho_r)\chi_r^2 + \mathcal{O}(\chi_r^3)$, with $\chi_r = (\rho - \rho_r)/(3\rho_r)$. Setting $\rho_r = \rho_0$ leads to the conventional $L \equiv L(\rho_0)$ and $K_{\rm sym} \equiv K_{\rm sym}(\rho_0)$.

Within the eSHF model [32,33] which includes 13 Skyrme interaction parameters α, $t_0 \sim t_5$, $x_0 \sim x_5$ and the spin-orbit coupling constant W_0, we have

$$\begin{aligned} E_0(\rho) = {} & \frac{3\hbar^2}{10m}k_F^2 + \frac{3}{8}t_0\rho + \frac{3}{80}[3t_1 + t_2(4x_2 + 5)]\rho k_F^2 \\ & + \frac{1}{16}t_3\rho^{\alpha+1} + \frac{3}{80}[3t_4 + t_5(4x_5 + 5)]\rho^2 k_F^2, \end{aligned} \tag{2}$$

and

$$\begin{aligned} E_{\rm sym}(\rho) = {} & \frac{\hbar^2}{6m}k_F^2 - \frac{1}{8}t_0(2x_0 + 1)\rho - \frac{1}{48}t_3(2x_3 + 1)\rho^{\alpha+1} \\ & - \frac{1}{24}[3t_1x_1 - t_2(4 + 5x_2)]\rho k_F^2 \\ & - \frac{1}{24}[3t_4x_4 - t_5(4 + 5x_5)]\rho^2 k_F^2, \end{aligned} \tag{3}$$

where m is the nucleon rest mass and $k_F = (3\pi^2/2\rho)^{1/3}$ is the Fermi momentum. The last term in Eqs. (2) and (3) is from the momentum dependence of three-body forces which is not considered in the standard SHF model (see, e.g., Ref. [34]). The eSHF provides a successful framework to describe simultaneously nuclear matter, finite nuclei, and NSs [33]. The 13 Skyrme parameters α, $t_0 \sim t_5$, $x_0 \sim x_5$ can be expressed explicitly in terms of the following 13 macroscopic quantities (pseudoparameters) [33]: ρ_0, $E_0(\rho_0)$, K_0, J_0, $E_{\rm sym}(\rho_r)$, $L(\rho_r)$, $K_{\rm sym}(\rho_r)$, the isoscalar effective mass $m^*_{s,0}$, the isovector effective mass $m^*_{v,0}$, the gradient coefficient G_S, and the symmetry-gradient coefficient G_V, the cross gradient coefficient G_{SV}, and the Landau parameter G'_0 of SNM in the spin-isospin channel. Instead of directly using the 13 Skyrme parameters, we use here the 13 macroscopic model parameters in the eSHF calculations for nuclear matter, finite nuclei, and NSs [33].

For NSs, we consider the conventional NS model, i.e., the NS contains core, inner crust, and outer crust with the core including only neutrons, protons, electrons, and possible muons ($npe\mu$). For the details, one is referred to Refs. [23,24,33]. We emphasize that in the following NS calculations, the core EOS is obtained from full eSHF calculations with model parameters constrained by properties of both finite nuclei and NSs as well as HIC flow data, and the core-crust transition density ρ_t is determined self-consistently by a dynamical approach [35]. In addition, all the constructed eSHF parameter sets used in the following NS calculations are required to satisfy the causality condition.

Result and discussion. For the 13 macroscopic model parameters in eSHF, we fix $E_{\rm sym}(\rho_c) = 26.65$ MeV since it has been obtained with high precision by analyzing the binding energy difference of heavy isotope pairs [20]. Furthermore, the L_c essentially determines the $\Delta r_{\rm np}$ of heavy nuclei [20], while the higher-order parameters J_0 and $K_{\rm sym}$ only weakly affect the properties of finite nuclei but are critical for NS properties [23,24]. To explore the $\Delta r_{\rm np}$ and NSs, therefore, our strategy is to search for the parameter space of L_c, J_0, and $K_{\rm sym}$ under the constraints on the SNM EOS from flow data as well as the limits from GW170817 and NS observations, while with the other 10 parameters [ρ_0, $E_0(\rho_0)$, K_0, $m^*_{s,0}$, $m^*_{v,0}$, G_S, G_V, G_{SV}, G'_0, and W_0] being obtained by fitting the nuclear data on the binding energies, charge rms radii, GMR energies, and spin-orbit energy level splittings (see Refs. [23,24,33] for details) to guarantee that the eSHF can successfully describe nuclear properties (the relative deviations of charge radii and total binding energies for medium and heavy nuclei from data are less than 0.5%). From the obtained L_c, J_0, and $K_{\rm sym}$, one can extract information on EOS, $\Delta r_{\rm np}$, and NSs.

A larger L_c generally leads to a larger $\Delta r_{\rm np}^{208}$ and correspondingly a larger $\Lambda_{1.4}$. For fixed L_c and J_0, reducing the $K_{\rm sym}$ can effectively reduce the $\Lambda_{1.4}$ but also reduces the NS maximum mass $M_{\rm max}$ [23,24]. Furthermore, increasing J_0 can enhance significantly the $M_{\rm max}$ but the J_0 cannot be too large [23,24,28] due to relatively soft SNM EOS constrained by the flow data. Using the limit of $\Lambda_{1.4} \leqslant 580$ from GW170817, $M_{\rm max} \geqslant 2.05M_\odot$ from PSR J0740+6620, and the flow data constraint on SNM EOS, one thus expects there should exist an upper limit for L_c (also for J_0 and $K_{\rm sym}$). Figures 1(a), 1(b) and 1(c) show the $M_{\rm max}$ vs $K_{\rm sym}$ at various J_0 with $L_c = 57$, 65, and 73 MeV, respectively. The shadowed regions represent the allowed parameter space of J_0 and $K_{\rm sym}$, which all satisfy the limits of $\Lambda_{1.4} \leqslant 580$, $M_{\rm max} \geqslant 2.05M_\odot$, and the flow data constraint. We note that the allowed parameter space agrees with $\Delta r_{\rm np}^{208} \geqslant 0.212$ fm. As expected, one sees from Fig. 1

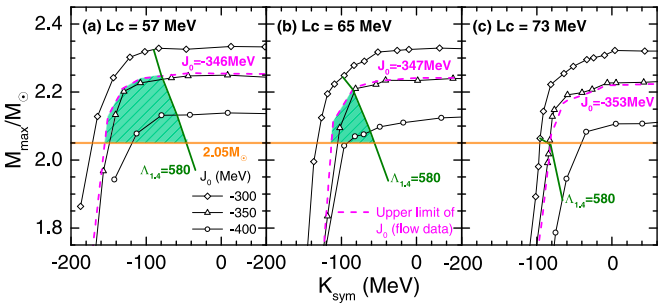

FIG. 1. NS maximum mass $M_{\rm max}$ vs $K_{\rm sym}$ within the eSHF model in a series of extended Skyrme interactions with J_0 and $K_{\rm sym}$ fixed at various values for $L_c = 57$ MeV (a), 65 MeV (b), and 73 MeV (c), respectively. The shadowed regions indicate the allowed parameter space. See the text for details.

that the allowed parameter space becomes smaller and smaller with increasing L_c (see also Ref. [24]), and it is essentially reduced to a point at $L_c = 73$ MeV with $K_{\rm sym} = -82$ MeV and $J_0 = -353$ MeV as shown in Fig. 1(c) (the corresponding parameter set is denoted as "Lc73"). Therefore, our results indicate the L_c has an upper limit of $L_c \leqslant 73$ MeV.

We note that the eSHF with Lc73 predicts $\Delta r_{\rm np}^{208} = 0.268$ fm, which is consistent with the $\Delta r_{\rm np}^{208} = 0.283 \pm 0.071$ fm from PREX-II. On the other hand, a smaller L_c will lead to a smaller $\Delta r_{\rm np}^{208}$ and thus may violate the constraint $\Delta r_{\rm np}^{208} = 0.283 \pm 0.071$ fm. Therefore, the lower limit of $\Delta r_{\rm np}^{208} = 0.212$ fm from PREX-II can set a lower limit of L_c. To obtain a quantitative relation between L_c and $\Delta r_{\rm np}^{208}$, we construct a series of parameter sets with L_c from 30 to 90 MeV in a step of 5 MeV. For the nine parameter sets of $L_c = 30$–70 MeV, the J_0 and $K_{\rm sym}$ are obtained by requiring them to reach the largest NS mass under the constraints of $\Lambda_{1.4} \leqslant 580$ and $M_{\rm max} \geqslant 2.05 M_\odot$ as well as the flow data constraints on SNM EOS. For the 4 parameter sets of $L_c = 75$–90 MeV, the constraint of $\Lambda_{1.4} \leqslant 580$ is turned off since it cannot be satisfied for $L_c \geqslant 75$ MeV under the constraints of $M_{\rm max} \geqslant 2.05 M_\odot$ and the flow data as discussed earlier.

Using the constructed 13 parameter sets, we plot the L_c vs $\Delta r_{\rm np}^{208}$ in Fig. 2(a). As expected, the L_c displays a very strong

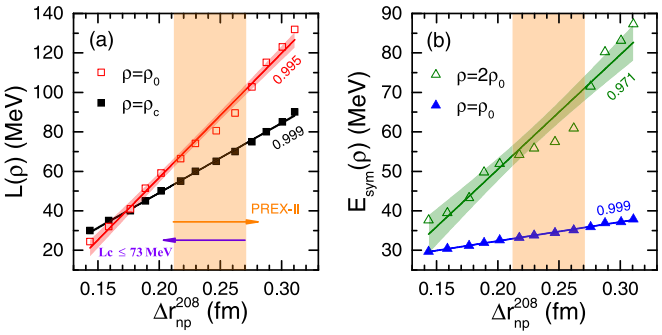

FIG. 2. The correlation of $\Delta r_{\rm np}^{208}$ with L_c and L (a) as well as $E_{\rm sym}(\rho_0)$ and $E_{\rm sym}(2\rho_0)$ (b) in the eSHF model. The limit of $0.212 \leqslant \Delta r_{\rm np}^{208} \leqslant 0.271$ fm from PREX-II [1] and $L_c \leqslant 73$ MeV obtained in this work is indicated by the orange band.

positive linear correlation with $\Delta r_{\rm np}^{208}$, i.e.,

$$L_c = (-21.65 \pm 1.02) + (353.78 \pm 4.32)\Delta r_{\rm np}^{208} \quad (4)$$

or

$$\Delta r_{\rm np}^{208} = (0.0615 \pm 0.0022) + (0.00282 \pm 0.0000344) L_c, \quad (5)$$

where the units of L_c and $\Delta r_{\rm np}^{208}$ are MeV and fm, respectively. Using Eq. (4), one obtains a lower limit of $L_c = 52.0$ MeV with $\Delta r_{\rm np}^{208} = 0.212$ fm. It is interesting to note that using $L_c = 73$ MeV in Eq. (5) leads to an upper limit of $\Delta r_{\rm np}^{208} = 0.271$ fm, nicely consistent with the eSHF prediction with Lc73. We thus conclude $0.212 \leqslant \Delta r_{\rm np}^{208} \leqslant 0.271$ fm and correspondingly $52 \leqslant L_c \leqslant 73$ MeV.

To see the implications of the constraint $0.212 \leqslant \Delta r_{\rm np}^{208} \leqslant 0.271$ fm on the symmetry energy, we also show in Fig. 2 the $\Delta r_{\rm np}^{208}$ vs L, $E_{\rm sym}(\rho_0)$, and $E_{\rm sym}(2\rho_0)$, which all display strong linear correlations. To understand these correlations, it is instructive to write down

$$L(\rho_r) \approx L\rho_r/\rho_0 + K_{\rm sym}\rho_r/\rho_0(\rho_r - \rho_0)/(3\rho_0), \quad (6)$$

by using $E_{\rm sym}(\rho) \approx E_{\rm sym}(\rho_0) + L\chi + \frac{1}{2!}K_{\rm sym}\chi^2$, which is a very good approximation to $E_{\rm sym}(\rho)$ for density less than about $2\rho_0$ [36,37]. Taking $\rho_c = 0.11$ fm$^{-3} \approx 2/3\rho_0$, one can obtain the following relations

$$L \approx 3L_c/2 + K_{\rm sym}/9, \quad (7)$$

$$E_{\rm sym}(\rho_0) \approx E_{\rm sym}(\rho_c) + L_c/6 + K_{\rm sym}/162, \quad (8)$$

$$E_{\rm sym}(2\rho_0) \approx E_{\rm sym}(\rho_c) + 2L_c/3 + 8K_{\rm sym}/81, \quad (9)$$

which indicate the L, $E_{\rm sym}(\rho_0)$, and $E_{\rm sym}(2\rho_0)$ are all linearly correlated with L_c (and thus $\Delta r_{\rm np}^{208}$) for fixed $E_{\rm sym}(\rho_c)$ and small disturbance from $K_{\rm sym}$. From the strong linear correlations shown in Fig. 2, one obtains $L = 83.1 \pm 24.7$ MeV, $E_{\rm sym}(\rho_0) = 34.3 \pm 1.7$ MeV, and $E_{\rm sym}(2\rho_0) = 62.8 \pm 15.9$ MeV. These results suggest a rather stiff symmetry energy around ρ_0, in contrast to the constraints $E_{\rm sym}(\rho_0) = 31.6 \pm 2.7$ MeV and $L = 58.9 \pm 16$ MeV [38,39], or $E_{\rm sym}(\rho_0) = 31.7 \pm 3.2$ MeV and $L = 58.7 \pm 28.1$ MeV [40], and $E_{\rm sym}(2\rho_0) = 47^{+23}_{-22}$ MeV [41], obtained by averaging essentially all the existing constraints. In addition, *ab initio* coupled-cluster calculations [42] predict a rather soft symmetry energy of $37.8 \leqslant L \leqslant 47.7$ MeV and $25.2 \leqslant E_{\rm sym}(\rho_0) \leqslant 30.4$ MeV, which are significantly smaller than our present constraints. It is interesting to mention that the present constraints are in surprisingly good agreement with the earlier constraint $L = 88 \pm 22$ MeV [16] obtained from transport model analyses [43,44] on the isospin diffusion data [45] in heavy-ion collisions, as well as the constraints $E_{\rm sym}(\rho_0) = 35.0 \pm 1.5$ MeV and $L = 85.5 \pm 15.5$ MeV obtained from the analyses of isovector skin and isobaric analog states [46].

Figure 3 shows the correlation of $\Delta r_{\rm np}^{208}$ with the crust-core transition density ρ_t, the threshold density $\rho_{\rm DU}$ and threshold NS mass $M_{\rm DU}$ above which the direct Urca (DU) process ($n \to p + e^- + \bar{\nu}_e$, $p + e^- \to n + \nu_e$) [47] becomes possible, the radius R_M of NS with mass $M = 1.0 M_\odot$, $1.4 M_\odot$, and $1.6 M_\odot$ as well as $M = 1.34 M_\odot$ and $1.44 M_\odot$. One sees the

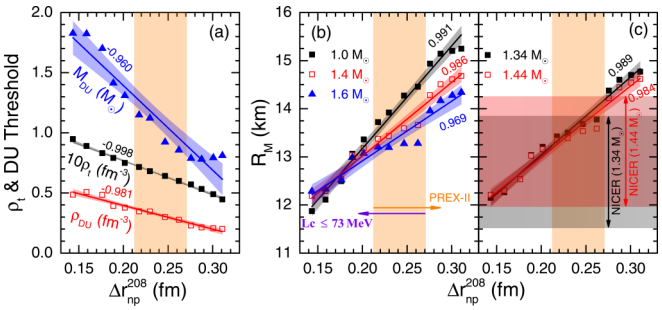

FIG. 3. Same as Fig. 2 but for the correlation with ρ_t, $\rho_{\rm DU}$, and $M_{\rm DU}$ (a); the radius R_M of NS with mass $M = 1.0M_\odot$, $1.4M_\odot$, and $1.6M_\odot$ (b); and the R_M with $M = 1.34M_\odot$ and $1.44M_\odot$ (c). The NICER constraints [29,30] are also included in panel (c) for comparison.

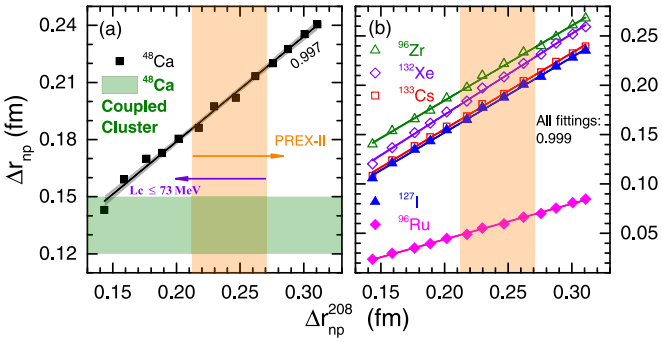

FIG. 4. Same as Fig. 2 but for the correlation with $\Delta r_{\rm np}$ of ^{48}Ca (a) and ^{96}Zr, ^{96}Ru, ^{127}I, ^{133}Cs, and ^{132}Xe (b). The $\Delta r_{\rm np}$ of ^{48}Ca from *ab initio* coupled-cluster calculations [42] is also included in panel (a) for comparison.

$\Delta r_{\rm np}^{208}$ exhibits a strong linear (anti-)correlation with all these NS properties, which together with the constraint $0.212 \leqslant \Delta r_{\rm np}^{208} \leqslant 0.271$ fm allow us to obtain following information: $\rho_t = 0.065 \pm 0.010$ fm^{-3}, $\rho_{\rm DU} = 0.313 \pm 0.096$ fm^{-3}, $M_{\rm DU} = (1.09 \pm 0.41)M_\odot$, $R_{1.0} = 14.07 \pm 0.91$ km, $R_{1.4} = 13.66 \pm 0.71$ km, $R_{1.6} = 13.44 \pm 0.68$ km, $R_{1.34} = 13.72 \pm 0.72$ km, and $R_{1.44} = 13.62 \pm 0.70$ km. Our results suggest a relatively small ρ_t, implying the NS crust will have a small thickness, fractional mass, and moment of inertia [35]. The $M_{\rm DU} = (1.09 \pm 0.41)M_\odot$ and $\rho_{\rm DU} = 0.313 \pm 0.096$ fm^{-3} indicate that the DU process will clearly occur in NSs with mass larger than $1.50M_\odot$ (central density larger than 0.409 fm^{-3}). Furthermore, if $\Delta r_{\rm np}^{208}$ were larger than 0.25 fm, one obtains $M_{\rm DU} \lesssim 1.0M_\odot$, and this means the DU process will occur in essentially all the observed NSs. The DU process will enhance the emission of neutrinos and make it a more important process in the cooling of a NS [47]. This observation is particularly interesting given the fact that a fast neutrino-cooling process has been suggested by the detected x-ray spectrum of the NS in the low-mass x-ray binary MXB 1659-29 [48]. Nevertheless, it should be mentioned that the NS cooling can be significantly influenced by nucleon pairing [49,50].

As for the NS radii, very strong limits with a precision of 5% have been obtained. In particular, our present results $R_{1.34} = 13.72 \pm 0.72$ km and $R_{1.44} = 13.62 \pm 0.70$ km are in agreement with the NICER constraints [29,30] but have much better precision. It is interesting to point out that the NICER constraints have not been imposed in constructing the parameter sets of $L_c = 30$–90 MeV, implying in eSHF, they are compatible with $\Lambda_{1.4} \leqslant 580$ and $M_{\rm max} \geqslant 2.05M_\odot$ as well as the flow data constraints on SNM EOS. It should be noted that the NS radius depends on the poorly known inner crust EOS [35,51] but $\Lambda_{1.4}$ does not [23], and thus it is relatively safer to use $\Lambda_{1.4}$ as a constraint.

Shown in Fig. 4 is the $\Delta r_{\rm np}^{208}$ vs the $\Delta r_{\rm np}$ of ^{48}Ca, ^{96}Zr, ^{96}Ru, ^{127}I, ^{133}Cs, and ^{132}Xe, and very strong positive linear correlations are seen between the $\Delta r_{\rm np}$ of these nuclei. Using $0.212 \leqslant \Delta r_{\rm np}^{208} \leqslant 0.271$ fm together with the linear correlations, we obtain $\Delta r_{\rm np}^{48}({\rm Ca}) = 0.202 \pm 0.020$ fm for ^{48}Ca, $\Delta r_{\rm np}^{96}({\rm Zr}) = 0.216 \pm 0.025$ fm for ^{96}Zr, $\Delta r_{\rm np}^{96}({\rm Ru}) = 0.059 \pm 0.012$ fm for ^{96}Ru, $\Delta r_{\rm np}^{127}({\rm I}) = 0.184 \pm 0.025$ fm for ^{127}I, $\Delta r_{\rm np}^{133}({\rm Cs}) = 0.187 \pm 0.025$ fm for ^{133}Cs, and $\Delta r_{\rm np}^{132}({\rm Xe}) = 0.204 \pm 0.027$ fm for ^{132}Xe.

Particularly interesting is the $\Delta r_{\rm np}^{48}({\rm Ca})$ as it has been predicted to be $0.12 \leqslant \Delta r_{\rm np}^{48}({\rm Ca}) \leqslant 0.15$ fm from *ab initio* coupled-cluster calculations [42], which is significantly smaller than our result $\Delta r_{\rm np}^{48}({\rm Ca}) = 0.202 \pm 0.020$ fm. At this point, we must mention that the Calcium Radius EXperiment (CREX) [1] is expected to finish the data analysis on $\Delta r_{\rm np}^{48}({\rm Ca})$ soon with a precision of 0.5% (or ± 0.02 fm) for its r_n. CREX can thus provide a unique bridge between *ab initio* approaches and density-functional theory (DFT). This is particularly important as the DFT (e.g., eSHF) is still the only realistic framework to investigate the physics of heavy nuclei and NSs.

The $\Delta r_{\rm np}^{96}({\rm Zr})$ and $\Delta r_{\rm np}^{96}({\rm Ru})$ are also very interesting since a recent study [52] has demonstrated that the isobaric ^{96}Zr + ^{96}Zr and ^{96}Ru + ^{96}Ru collisions at relativistic energies can be used to extract the $\Delta r_{\rm np}$ of ^{96}Zr and ^{96}Ru with a weak model dependence. The $\Delta r_{\rm np}^{96}({\rm Zr})$ and $\Delta r_{\rm np}^{96}({\rm Ru})$ are also crucial for the chiral magnetic effect search in isobaric collisions [53]. Our present results of $\Delta r_{\rm np}^{96}({\rm Zr})$ and $\Delta r_{\rm np}^{96}({\rm Ru})$ are particularly timely, because the data on these isobaric collisions at RHIC have been taken in 2018 and have been subject to a blinded analysis to assess the chiral magnetic effect. In addition, our results of $\Delta r_{\rm np}^{127}({\rm I})$ and $\Delta r_{\rm np}^{133}({\rm Cs})$ are critical for the information extraction of new physics [6] via coherent elastic neutrino-nucleus scattering in the COHERENT experiment [4], while the $\Delta r_{\rm np}^{132}({\rm Xe})$ is important for dark matter direct detection in liquid Xe detector [54].

Finally, it is instructive to see how our results change if the adopted constraints are varied. We note the upper limit of L_c changes from 73 MeV to 82 MeV if the $\Lambda_{1.4} \leqslant 580$ [25] is altered into $\Lambda_{1.4} \leqslant 720$ which seems to be favored if a NS maximum mass of $1.97M_\odot$ is imposed in the analysis of GW170817 [55]. In addition, varying the $M_{\rm max} \geqslant 2.05M_\odot$ [26] into the recently updated $M_{\rm max} \geqslant 2.01M_\odot$ [56] from PSR J0740+6620 only changes $L_c \leqslant 73$ MeV to $L_c \leqslant 74$ MeV, enhancing the pressure upper limit of SNM EOS constraint from the flow data by 10% essentially does not change the limit $L_c \leqslant 73$ MeV, and replacing $E_{\rm sym}(\rho_c) = 26.65$ MeV by $E_{\rm sym}(\rho_c) = 25.65(27.65)$ MeV leads to $L_c \leqslant 69(75)$ MeV. We also note replacing $\Lambda_{1.4} \leqslant 580$ by $\Lambda_{1.4} \leqslant$

720 leads to $0.212 \leqslant \Delta r_{\rm np}^{208} \leqslant 0.288$ fm, $E_{\rm sym}(\rho_0) = 34.8 \pm 2.1$ MeV, $L(\rho_0) = 89.0 \pm 30.6$ MeV, and $E_{\rm sym}(2\rho_0) = 65.7 \pm 18.7$ MeV. At last, it should be noted that the present results are based on the conventional NS model in a single unified framework without considering possible new degrees of freedom (hyperons, meson condensates, quark matter, and so on) and modified gravity.

Conclusion. We have demonstrated the symmetry energy slope parameter L_c cannot be larger than 73 MeV under the condition of $\Lambda_{1.4} \leqslant 580$, and this leads to an upper limit of $\Delta r_{\rm np}^{208} \leqslant 0.271$ fm. This limit together with the recent model-independent measurement on $\Delta r_{\rm np}^{208}$ from PREX-II leads to a rather large but very precise constraint of $0.212 \leqslant \Delta r_{\rm np}^{208} \leqslant 0.271$ fm, which suggests a rather stiff symmetry energy around ρ_0 and has critical implications on many issues in nuclear physics and astrophysics. In particular, our present constraints on the symmetry energy and the neutron skin of ^{48}Ca reveal serious tension with the predictions from *ab initio* coupled-cluster theory, and the soon coming data from CREX thus become extremely important.

Acknowledgments. This work was supported by National SKA Program of China No. 2020SKA0120300 and the National Natural Science Foundation of China under Grants No. 11625521 and No. 11905302.

[1] D. Adhikari *et al.* (PREX Collaboration), Accurate Determination of the Neutron Skin Thickness of ^{208}Pb Through Parity-Violation in Electron Scattering, Phys. Rev. Lett. **126**, 172502 (2021).

[2] S. Abrahamyan *et al.* (PREX Collaboration), Measurement of the Neutron Radius of ^{208}Pb Through Parity Violation in Electron Scattering, Phys. Rev. Lett. **108**, 112502 (2012).

[3] D. Becker *et al.*, The P2 experiment - A future high-precision measurement of the weak mixing angle at low momentum transfer, Eur. Phys. J. A **54**, 208 (2018).

[4] D. Akimov *et al.* (COHERENT Collaboration), Observation of coherent elastic neutrino-nucleus scattering, Science **357**, 1123 (2017).

[5] M. Cadeddu, C. Giunti, Y. F. Li, and Y. Y. Zhang, Average CsI Neutron Density Distribution from COHERENT Data, Phys. Rev. Lett. **120**, 072501 (2018).

[6] X. R. Huang and L. W. Chen, Neutron skin in CsI and low-energy effective weak mixing angle from COHERENT data, Phys. Rev. D **100**, 071301(R) (2019).

[7] M. Thiel, C. Sfienti, J. Piekarewicz, C. J. Horowitz, and M. Vanderhaeghen, Neutron skins of atomic nuclei: Per aspera ad astra, J. Phys. G: Nucl. Part. Phys. **46**, 093003 (2019).

[8] A. W. Steiner, M. Prakash, J. M. Lattimer, and P. J. Ellis, Isospin asymmetry in nuclei and neutron stars, Phys. Rep. **411**, 325 (2005).

[9] B. A. Li, L. W. Chen, and C. M. Ko, Recent progress and new challenges in isospin physics with heavy-ion reactions, Phys. Rep. **464**, 113 (2008).

[10] S. Gandolfi, A. Gezerlis, and J. Carlson, Neutron matter from low to high density, Annu. Rev. Nucl. Part. Sci. **65**, 303 (2015).

[11] N. B. Zhang and B. A. Li, Extracting nuclear symmetry energies at high densities from observations of neutron stars and gravitational waves, Eur. Phys. J. A **55**, 39 (2019).

[12] F. Özel, and P. Freire, Masses, radii, and the equation of state of neutron stars, Annu. Rev. Astron. Astrophys. **54**, 401 (2016).

[13] M. Baldo and G. F. Burgio, The nuclear symmetry energy, Prog. Part. Nucl. Phys. **91**, 203 (2016).

[14] B. Alex Brown, Neutron Radii in Nuclei and the Neutron Equation of Wtate, Phys. Rev. Lett. **85**, 5296 (2000).

[15] R. J. Furnstahl, Neutron radii in mean-field models, Nucl. Phys. A **706**, 85 (2002).

[16] L. W. Chen, C. M. Ko, and B. A. Li, Nuclear matter symmetry energy and the neutron skin thickness of heavy nuclei, Phys. Rev. C **72**, 064309 (2005).

[17] M. Centelles, X. Roca-Maza, X. Vinas, and M. Warda, Nuclear Symmetry Energy Probed by Neutron Skin Thickness of Nuclei, Phys. Rev. Lett. **102**, 122502 (2009).

[18] L. W. Chen, C. M. Ko, B.-A. Li, and J. Xu, Density slope of the nuclear symmetry energy from the neutron skin thickness of heavy nuclei, Phys. Rev. C **82**, 024321 (2010).

[19] X. Roca-Maza, M. Centelles, X. Vinas, and M. Warda, Neutron Skin of ^{208}Pb, Nuclear Symmetry Energy, and the Parity Radius Experiment, Phys. Rev. Lett. **106**, 252501 (2011).

[20] Z. Zhang and L. W. Chen, Constraining the symmetry energy at subsaturation densities using isotope binding energy difference and neutron skin thickness, Phys. Lett. B **726**, 234 (2013).

[21] B. G. Todd-Rutel and J. Piekarewicz, Neutron-Rich Nuclei and Neutron Stars: A New Accurately Calibrated Interaction for the Study of Neutron-Rich Matter, Phys. Rev. Lett. **95**, 122501 (2005).

[22] F. J. Fattoyev, J. Piekarewicz, and C. J. Horowitz, Neutron Skins and Neutron Stars in the Multimessenger Era, Phys. Rev. Lett. **120**, 172702 (2018).

[23] Y. Zhou, L. W. Chen, and Z. Zhang, Equation of state of dense matter in the multimessenger era, Phys. Rev. D **99**, 121301(R) (2019).

[24] Y. Zhou and L. W. Chen, Ruling out the supersoft high-density symmetry energy from the discovery of PSR J0740+6620 with Mass $2.14^{+0.10}_{-0.09} M_\odot$, Astrophys. J. **886**, 52 (2019).

[25] B. P. Abbott *et al.*, GW170817: Measurements of Neutron Star Radii and Equation of State, Phys. Rev. Lett. **121**, 161101 (2018).

[26] H. T. Cromartie *et al.*, Relativistic Shapiro delay measurements of an extremely massive millisecond pulsar, Nat. Astron. **4**, 72 (2020).

[27] P. Danielewicz, R. Lacey, and W. G. Lynch, Determination of the equation of state of dense matter, Science **298**, 1592 (2002).

[28] B. J. Cai and L. W. Chen, Constraints on the skewness coefficient of symmetric nuclear matter within the nonlinear relativistic mean field model, Nucl. Sci. Tech. **28**, 185 (2017).

[29] T. E. Riley *et al.*, A NICER View of PSR J0030+0451: Millisecond pulsar parameter estimation, Astrophys. J. Lett. **887**, L21 (2019).

[30] M. C. Miller *et al.*, PSR J0030+0451 mass and radius from NICER data and implications for the properties of neutron star matter, Astrophys. J. Lett. **887**, L24 (2019).

[31] B. T. Reed, F. J. Fattoyev, C. J. Horowitz, and J. Piekarewicz, Implications of PREX-II on the Equation of

State of Neutron-Rich Matter, Phys. Rev. Lett. **126**, 172503 (2021).

[32] N. Chamel, S. Goriely, and J. M. Pearson, Further explorations of Skyrme-Hartree-Fock-Bogoliubov mass formulas. XI. Stabilizing neutron stars against a ferromagnetic collapse, Phys. Rev. C **80**, 065804 (2009).

[33] Z. Zhang and L. W. Chen, Extended Skyrme interactions for nuclear matter, finite nuclei, and neutron stars, Phys. Rev. C **94**, 064326 (2016).

[34] E. Chabanat *et al.*, A Skyrme parametrization from subnuclear to neutron star densities, Nucl. Phys. A **627**, 710 (1997).

[35] J. Xu, L. W. Chen, B. A. Li, and H. R. Ma, Nuclear constraints on properties of neutron star crusts, Astrophys. J. **697**, 1549 (2009).

[36] L. W. Chen, B. J. Cai, C. M. Ko, B. A. Li, C. Shen, and J. Xu, Higher-order effects on the incompressibility of isospin asymmetric nuclear matter, Phys. Rev. C **80**, 014322 (2009).

[37] L. W. Chen, Higher order bulk characteristic parameters of asymmetric nuclear matter, Sci. China Phys. Mech. Astron. **54**, suppl.1, 124 (2011).

[38] B. A. Li and X. Han, Constraining the neutron-proton effective mass splitting using empirical constraints on the density dependence of nuclear symmetry energy around normal density, Phys. Lett. B **727**, 276 (2013).

[39] B. A. Li, P. G. Krastev, D. H. Wen, and N. B. Zhang, Towards understanding astrophysical effects of nuclear symmetry energy, Eur. Phys. J. A **55**, 117 (2019).

[40] M. Oertel, M. Hempel, T. Klahn, and S. Typel, Equations of state for supernovae and compact stars, Rev. Mod. Phys. **89**, 015007 (2017).

[41] W. J. Xie and B. A. Li, Bayesian inference of the symmetry energy of super-dense neutron-rich matter from future radius measurements of massive neutron stars, Astrophys. J. **899**, 4 (2020).

[42] G. Hagen *et al.*, Neutron and weak-charge distributions of the ^{48}Ca nucleus, Nat. Phys. **12**, 186 (2016).

[43] L. W. Chen, C. M. Ko, and B. A. Li, Determination of the Stiffness of the Nuclear Symmetry Energy from Isospin Diffusion, Phys. Rev. Lett. **94**, 032701 (2005).

[44] B. A. Li and L. W. Chen, Nucleon-nucleon cross sections in neutron-rich matter and isospin transport in heavy-ion reactions at intermediate energies, Phys. Rev. C **72**, 064611 (2005).

[45] M. B. Tsang *et al.*, Isospin Diffusion and the Nuclear Symmetry Energy in Heavy Ion Reactions, Phys. Rev. Lett. **92**, 062701 (2004).

[46] P. Danielewicz, P. Singh, and J. Lee, Symmetry energy III: Isovector skins, Nucl. Phys. A **958**, 147 (2017).

[47] J. M. Lattimer, C. J. Pethick, M. Prakash, and P. Haensel, Direct URCA Process in Neutron Stars, Phys. Rev. Lett. **66**, 2701 (1991).

[48] E. F. Brown, A. Cumming, F. J. Fattoyev, C. J. Horowitz, D. Page, and S. Reddy, Rapid Neutrino Cooling in the Neutron Star MXB 1659-29, Phys. Rev. Lett. **120**, 182701 (2018).

[49] A. Potekhin, A. Chugunov, and G. Chabrier, Thermal evolution and quiescent emission of transiently accreting neutron stars, Astron. Astrophys. **629**, A88 (2019).

[50] D. Page, J. M. Lattimer, M. Prakash, and A. W. Steiner, Stellar superfluids, Astrophys. J. **707**, 1131 (2009).

[51] M. Fortin, C. Providencia, A. R. Raduta, F. Gulminelli, J. L. Zdunik, P. Haensel, and M. Bejger, Neutron star radii and crusts: Uncertainties and unified equations of state, Phys. Rev. C **94**, 035804 (2016).

[52] H. Li, H.-J. Xu, Y. Zhou, X. Wang, J. Zhao, L. W. Chen, and F. Wang, Probing the Neutron Skin with Ultrarelativistic Isobaric Collisions, Phys. Rev. Lett. **125**, 222301 (2020).

[53] H.-J. Xu, X. Wang, H. Li, J. Zhao, Z.-W. Lin, C. Shen, and F. Wang, Importance of Isobar Density Distributions on the Chiral Magnetic Effect Search, Phys. Rev. Lett. **121**, 022301 (2018).

[54] H. Zheng, Z. Zhang, and L. W. Chen, Form factor effects in the direct detection of isospin-violating dark matter, J. Cosmol. Astropart. Phys. **08**, 011 (2014).

[55] https://dcc.ligo.org/LIGO-P1800115/public.

[56] E. Fonseca *et al.*, Refined mass and geometric measurements of the high-mass PSR J0740+6620, Astrophys. J. Lett. **915**, L12 (2021).